DOI: 10.1002/chem.200700364

Charge-Transfer Emission Involving Three-Coordinate Organoboron: V-Shape versus U-Shape and Impact of the Spacer on Dual Emission and Fluorescent Sensing

Dong-Ren Bai, Xiang-Yang Liu, and Suning Wang*[a]

Abstract: New V-shaped bifunctional organosilicon compounds that contain an electron acceptor, $B(Mes)_2$, and an electron donor, N(1-naph)Ph, with the formulae $Ph_2Si\{p\text{-}C_6H_4B(Mes)_2\}\{p\text{-}C_6H_4N(1\text{-naph})ph)\}$ (**1**), $Ph_2Si\{p\text{-}C_6H_4\text{-}(Mes)_2\}\{p\text{-biphenyl-N(1-naph)ph}\}$ (**2**), and $Si\{p\text{-}C_6H_4B(Mes)_2\}_2\{p\text{-}C_6H_4N(1\text{-naph})ph)\}_2$ (**3**) have been synthesized as model compounds for the investigation of through-space charge-transfer emission involving triarylboron and triarylamino centers. The photophysical properties of the new bifunctional organosilicon compounds are compared to two U-shaped compounds sBN and BN in which the boron acceptor and the amino donor groups are linked together by a rigid 1,10-naphthyl group. The results of our investigation establish that dual emission pathways, namely through-space donor-acceptor charge transfer and π–π* transitions coexist in the V-shaped molecules **1**–**3**, while charge transfer emission is dominant in the U-shaped molecules. It is found that depending on the geometry of the linker and the B···N separation distance, the compound either displays dual emission bands simultaneously or single emission band. In addition, the dual emission pathways in these molecules can be selectively switched on or off by using fluoride ions. The sensitivity of response to fluoride ions by these molecules is also found to be highly dependent on the geometry of the linker and the B···N separation distance. The V-shaped molecules are found to be "turn-on" sensors to fluorides with a much higher sensitivity than the U-shaped molecules.

Keywords: boron · charge transfer · fluorescence · fluorides · sensors

Introduction

A unique property of three-coordinate organoboron compounds is their ability to accept electrons through the empty p_π orbital on the boron center. This property has been exploited extensively and successfully for applications of three-coordinate organoboron compounds in nonlinear optical materials,[1] in organic light-emitting diodes (as electron transport and emitters)[2] and in fluorescent sensing.[3–4]

The majority of three-coordinate boron compounds that contain a donor group have the "linear" geometry **A** as shown in Scheme 1, in which the donor and the acceptor are connected together by a linear, and in most instances, conjugated spacer such as an aryl group. Such linear organoboron compounds usually display a highly efficient donor–acceptor charge-transfer emission.[1–4] Two examples of system **A** developed by our groups are sBNPB and BNPB[2k,l] shown in Scheme 1. In contrast to **A** is the U-shaped geometry **C** in which the donor and the acceptor are pendent groups attached to a 1,10-bis(aryl)naphthalene linker, an example of which, the BN compound, was reported recently by us.[4] We have observed that unlike the linear molecules that operate primarily on charge-transfer emission, the BN compound has two emission pathways, through-space charge transfer and π–π* transition localized on the triarylamino portion that can be reversibly and selectively switched on or off by the addition of F^-.[4] Encouraged by the unusual photophysical properties of the BN molecule and the various potential applications of such switchable dual emission systems, we have expanded our investigation to the V-shaped system **B** in which the spacer is an organosilicon unit that provides a greater rotational freedom to the donor and the acceptor groups than the naphthyl linker in system **C**. Three new **B**-type compounds (**1**–**3**) with different donor–acceptor separation distances and different numbers of chromophores have been synthesized and investigated. Furthermore, we have

[a] D.-R. Bai, Dr. X.-Y. Liu, Prof. S. Wang
Department of Chemistry, Queen's University
Kingston, Ontario, K7L 3N6 (Canada)
Fax: (+1) 613-533-6669
E-mail: wangs@chem.queensu.ca

Supporting information for this article is available on the WWW under http://www.chemeurj.org/ or from the author.

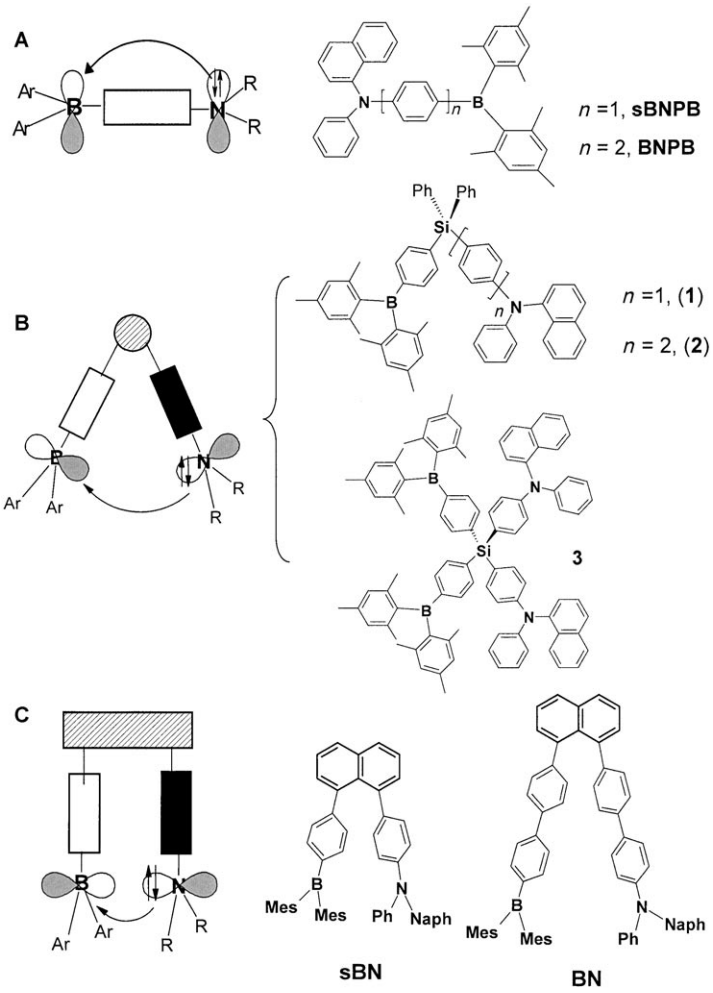

Scheme 1.

synthesized a new member of system **C**, compound sBN, a smaller version of BN. These new compounds along with BN allow us to conduct a comprehensive investigation on the impact of the geometry of the linker and the donor–acceptor separation distance on charge-transfer emission involving three-coordinate organoboron centers. The results are presented herein.

Results and Discussion

Syntheses: Three new organosilicon compounds **1**–**3** functionalized by $B(Mes)_2$ (acceptor) and N(1-naph)ph (donor) groups were designed and synthesized based on the following considerations. First, the Ph_2Si spacer provides more rotational freedom to the $(Mes)_2B$-aryl leg and the (1-naph)phN-aryl leg, compared to the 1,10-naphthyl spacer in the BN compound,[4] thus allowing us to investigate the impact of structural rigidity on charge-transfer emission in three-coordinate organoboron. Second, molecular modeling shows that the B···N separation distances in **1** and **2** are ≈10 and 14 Å, respectively, thus allowing us to examine the impact of donor–acceptor separation distance on charge-transfer emission in the V-shaped organoboron compounds. Third, although the B···N separation distance in **3** is about the same as that of **1**, the number of chromophores is doubled in **3**, thus allowing us to study the effect of the number of chromophores on through-space charge-transfer emission.

The synthetic procedure for the intermediates **1a**–**3a** and the final products **1**–**3** are shown in Scheme 2. The (1-naph)PhN-substituted intermediates **1a** and **3a** were synthesized by using a copper-catalyzed Ullmann condensation reaction[6] between an appropriate bromide and (1-nap)PhNH. These coupling reactions were found to be heavily affected by the reaction temperature. For example, when the reaction was carried out at 220 °C, **1a** was only obtained in 20% yield. At 230 °C, the yield of **1a** was doubled to 40%. Further increasing the reaction temperature to 240 °C increased the yield by another 5% . However at this temperature, the formation of the disubstituted product became evident, as revealed by mass spectroscopy. The synthesis of the intermediate **3a** was more challenging due to the formation of mono-, di-, tri-, and tetra-substituted products, which along with unreacted starting materials in the reaction mixture made the separation and purification of **3a** difficult. The similarity in polarity among the substituted products further complicated the product isolation. As a result, **3a** was only obtained in 25% yield. The boron-substituted intermediate **2a** was synthesized in 50% yield by lithiating di(*p*-bromophenyl)diphenylsilane, followed by the addition of $B(Mes)_2F$ at −78 °C. Compound **1** was synthesized by lithiating the intermediate **1a**, followed by the addition of $B(Mes)_2F$, a procedure similar to the synthesis of **2a**. However, we have observed that the halogen–metal exchange reaction at −78 °C only afforded 10% of **1** with most **1a** being recovered. Removing the dry-ice bath to allow the reaction mixture to reach ambient temperature slowly after *n*BuLi was added at −78 °C resulted in a fivefold increase in yield to 50%. Compound **2** was obtained by a Suzuki–Miyaura cross-coupling reaction[7] between **2a** and *p*-(1-naphthylphenylamino)phenylboronic acid in the presence of Na_2CO_3 as a base and by using $[Pd(PPh_3)_4]$ as the catalyst in 35% yield. Compound **3** was prepared in 70% yield by using a substitution reaction similar to that used for **1**. The U-shaped sBN molecule, a new member of system **C**, was synthesized according to Scheme 3. Among the various methods we tried, the best way for the synthesis of sBN is by lithiating *p*-I-C_6H_4-N(1-naph)Ph first, followed by the formation of the Zn^{II} complex and its cross-coupling to 1-I-8-*p*-{(mesityl)$_2$B}phenylnaphthalene (**4a**) in the presence of $[Pd(PPh_3)_4]$ at ambient temperature to produce sBN in ≈31% yield. Compounds **1**–**3** and sBN were fully characterized by NMR spectroscopy, HRMS, or elemental analyses.

UV/Vis absorption spectra: The absorption spectra of compounds **1**–**3** were examined in six representative solvents, namely hexane, toluene, CH_2Cl_2, THF, DMF, and CH_3CN. The data recorded in hexane, CH_2Cl_2, and DMF (1.0×10^{-5} M) for all three compounds along with BN, sBN, BNPB,

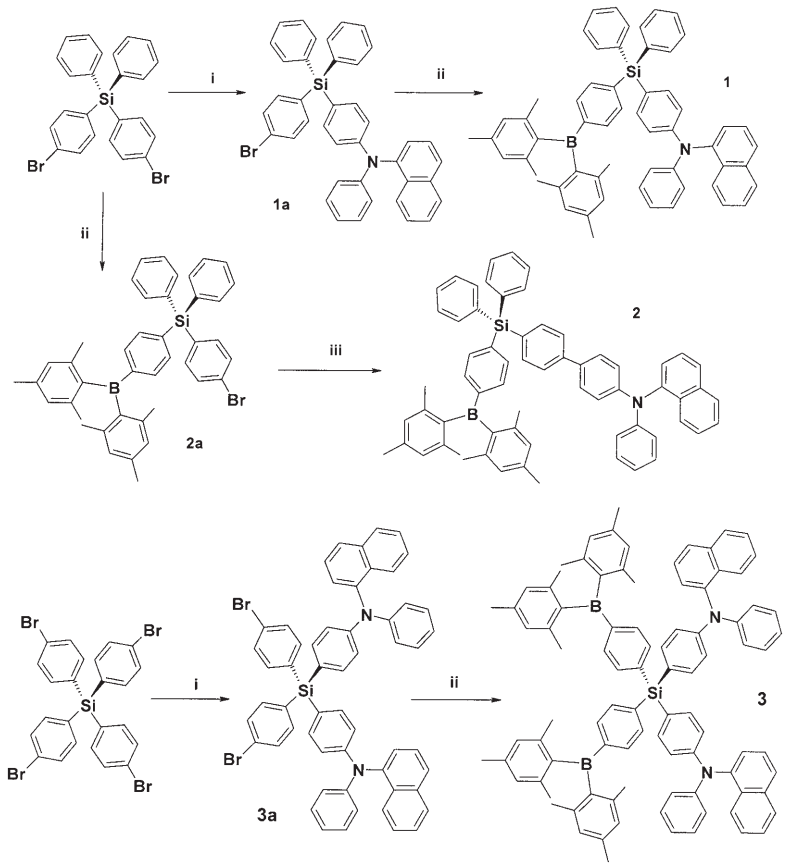

Scheme 2. i) HN(1-naph)Ph, 230–240 °C, CuSO4, K3PO4; ii) *n*BuLi, −78 °C; $BMes_2F$, RT; iii) (1-naph)PhN-*p*-phenyl-B(OH)2, $[Pd(PPh_3)_4]$, Na_2CO_3, reflux in toluene/ethanol/H_2O.

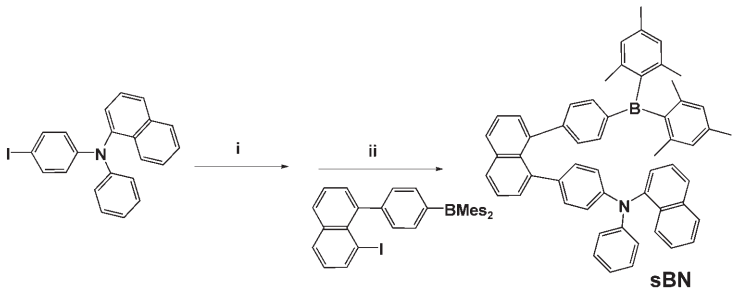

Scheme 3. i) *n*BuLi, $ZnCl_2$, −78 °C; ii) $[Pd(PPh_3)_4]$ at −30 °C.

and sBNPB are provided in Table 1 and shown in Figure 1. For comparison purpose, the spectra of **1** in various solvents are shown in Figure 2. The complete spectra for other compounds are provided in the Supporting Information.

The spectra of compounds **1–3** resemble those of sBN and BN. For **1** and **3**, the low energy absorption band appears at $\lambda max = \approx 310$ nm ($\log \varepsilon = 4.8$–5.1) covering the range of 260–390 nm. This absorption band is attributed to the charge-transfer transition between the N leg and the B leg and π–π* transitions localized on the leg. This absorption band does not change significantly with solvents as shown by Figure 2, a behavior resembling that of sBN and BN. Compounds **1** and **3** have nearly identical absorption spectra except that the absorption coefficient of the latter is about twice as large as the former; this result is consistent with the fact that the donor–acceptor distance in these two molecules are identical and there are two sets of chromophores in **3**. The absorption spectrum of **2** resembles those of **1** and **3** except that the λ_{max} of the low-energy band is red-shifted by about 15 nm ($\lambda_{max} = 325$ nm), attributable to the biphenyl group in **2** that effectively decreases the π–π* transition energy. Compared to the linear system **A** (sBNPB and BNPB), the λ_{max} of the low-energy band is blue shifted by 50–60 nm from **A** to **B**; this result accounts for the fact that system **A** compounds are light yellow, while system **B** compounds are all colorless.

Electrochemical properties: The redox properties of compounds **1–3** were examined by using cyclic voltammetry and compared to sBN and BN and the linear molecule BNPB. The data are summarized in Table 2. All compounds display a reversible oxidation peak at ≈1.0 V (versus Ag/AgCl electrode), which is typical of oxidation of the (1-naph)PhN group and similar to the second oxidation potential of (1-naph)PhN-biphenyl-NPh(1-naph) (NPB; see Supporting Information). Compound **3** displays a shoulder oxidation peak in addition to the main oxidation peak, an indication that some weak electronic communication between the two amino centers is present. For the V-shaped silicon compounds **1–3**, no well-defined reduction peaks were observed. For the U-shaped compounds sBN and BN, a quasi-reversible reduction peak at −1.8 to −1.9 V was observed which is similar to that[2k] of the linear molecule BNPB, attributable to the reduction of the three-coordinate boron center (see Supporting Information). These data indicate that the linear system **A** and the U-shaped system **C** molecules provide more stability to the reduced boron center than the V-shaped system **B** does. The strong interleg π–π interaction in system **C** may play a role in the relatively

Table 1. Absorption and luminescent properties of **1**–**3**, sBN, BN, sBNPB, and BNPB.[a]

	Solvent	Absorp. λ_{max} [nm]	Log ε	λ_{ex} [nm]	λ_{em} [nm]	Φ
1	hexane	310	4.85	318	392	0.35
	CH_2Cl_2	308	4.86	320	507	0.27
	DMF	310	4.94	308	435	0.07
2	hexane	326	4.92	330	398	0.64
	CH_2Cl_2	328	4.77	334	436	0.36
	DMF	320	4.75	337	444	0.15
3	hexane	308	5.11	321	391	0.31
	CH_2Cl_2	308	5.11	319	508	0.27
	DMF	310	5.14	313	434	0.03
sBN	hexane	332	4.67	345	454	0.17
	CH_2Cl_2	334	4.48	339	507	0.19
	DMF	290, 330(sh)	4.78	359	528(5 min) 462(24 hr)	0.15
BN	hexane	330	5.01	335	454	0.23
	CH_2Cl_2	334	4.89	376	507	0.10
	DMF	334	4.70	340	528(5 min) 459(1 hr)	0.23
sBNPB	hexane	376	4.31	374	415	1.00
	CH_2Cl_2	374	4.45	374	459	0.62
	DMF	376	4.47	374	476	0.45
BNPB	hexane	374	4.68	378	418	1.00
	CH_2Cl_2	378	4.79	378	486	0.82
	DMF	382	4.72	378	513	0.48

[a] All spectra were recorded by using a solution of 1.0×10^{-5} M.

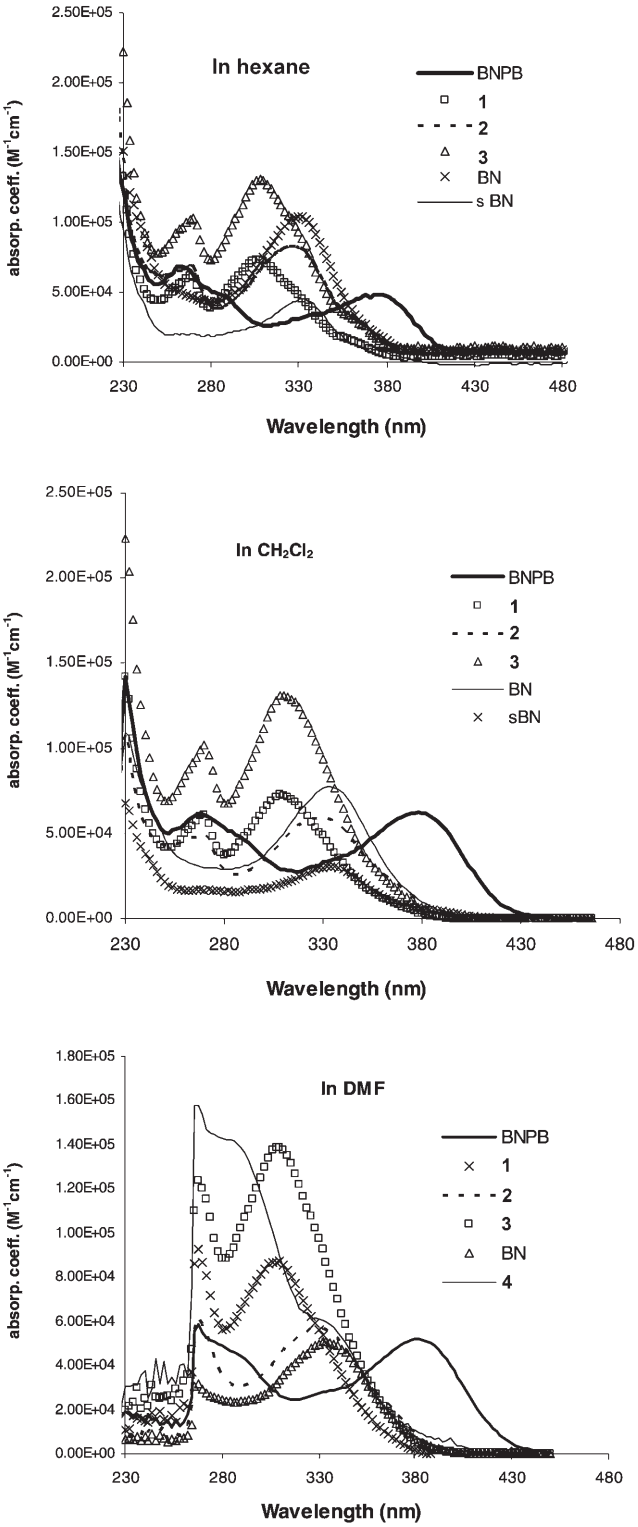

Figure 1. Absorption spectra in hexane (1.0×10^{-5} M) (top), in CH_2Cl_2 (1.0×10^{-5} M) (middle) and in DMF (1.0×10^{-5} M) (bottom).

higher stability of sBN and BN toward reduction, while the direct conjugation between the B center and the N center appears to be the key for the relative stability of system **A** molecules toward reduction. The redox potentials were converted to HOMO and LUMO energy after being calibrated using the $FeCp_2^+/FeCp_2$ as the standard.[8] LUMO energy levels for **1**–**3** were calculated by using the HOMO level and the optical band gap. As shown by the data in Table 2, the HOMO level changes little from system **A** to system **C**, while some variation of the LUMO level is apparent.

Molecular orbital calculations: Previously we have shown that for linear molecules in system **A** and the U-shaped molecules in system **C**, the HOMO level is dominated with contributions from the amino group, while the LUMO level is dominated by the empty p orbital of the boron center and as a consequence the lowest electronic transition in these molecules is B–N charge transfer. To determine if the silicon compounds **1**–**3** have a HOMO–LUMO profile similar to that of sBN and BN, we performed molecular orbital calculations for these molecules. Molecular modeling and geometric optimization were carried out to obtain geometric parameters for use in the calculation. The Gaussian suite of programs[9] (Gaussian 98) was employed. The calculations were performed with the 6–311G** basis set for all compounds. The orbital diagrams were generated by use of the Molekel program.[10] All contour values are ±0.025 au. The results of our calculations show that the HOMO level for all molecules consists of contributions from the N leg only, while the LUMO level involves contributions from the B leg only. For molecules **1**–**3**, the silicon center does not contribute to HOMO/LUMO at all. The second LUMO for all three molecules is a π^* orbital localized on the N leg. The MO diagrams for the HOMO, LUMO, and the second LUMO levels of **1** are shown in Figure 3 as a representative

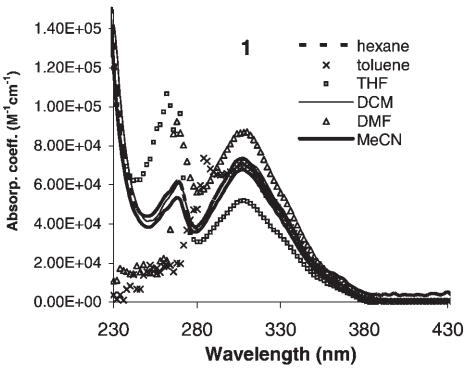

Figure 2. Absorption spectra of **1** in various solvents.

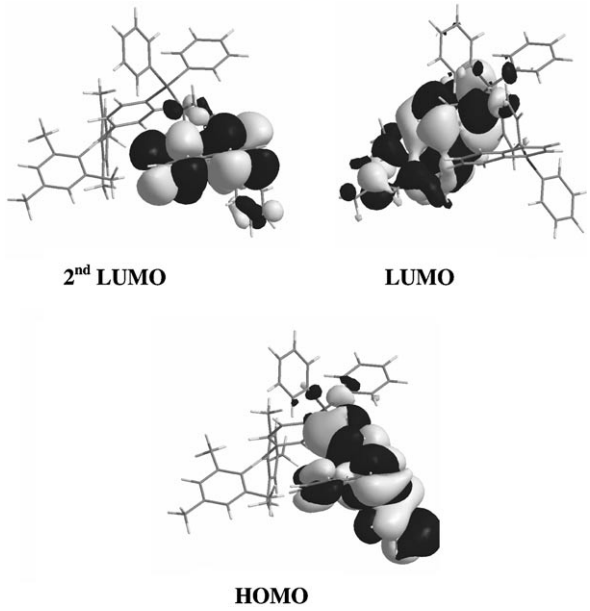

Figure 3. MO diagrams of **1**.

example. MO diagrams for other molecules can be found in the Supporting Information. Based on the MO results, the lowest electronic transition in these molecules can be assigned to charge transfer between the N leg and the B leg. The optimized geometry from MO calculations produced the B···N separation distance in **1**–**3**, sBN and BN to be 10.1, 13.9, 10.2, 6.7, and 9.7 Å, respectively.

Solvent-dependent emission: The linear molecule BNPB is known to display bright solvent-dependent luminescence when irradiated with UV light.[2k,l] The smaller linear molecule sBNPB shows similar solvent-dependent emission. The Stokes shift of these two linear molecules was found to have a linear relationship with the polarity of the solvents (see Supporting Information), consistent with charge-transfer emission and a highly polarized excited state.[1,11]

Compounds **1**–**3** also display solvent-dependent emission. The emission spectra of **1** and **3** are essentially identical, while the spectra of **2** are quite different as shown by Figure 4 (the emission spectra of **3** are provided in Supporting Information). At the first glance, the spectral shift of these compounds does not appear to have the same linear

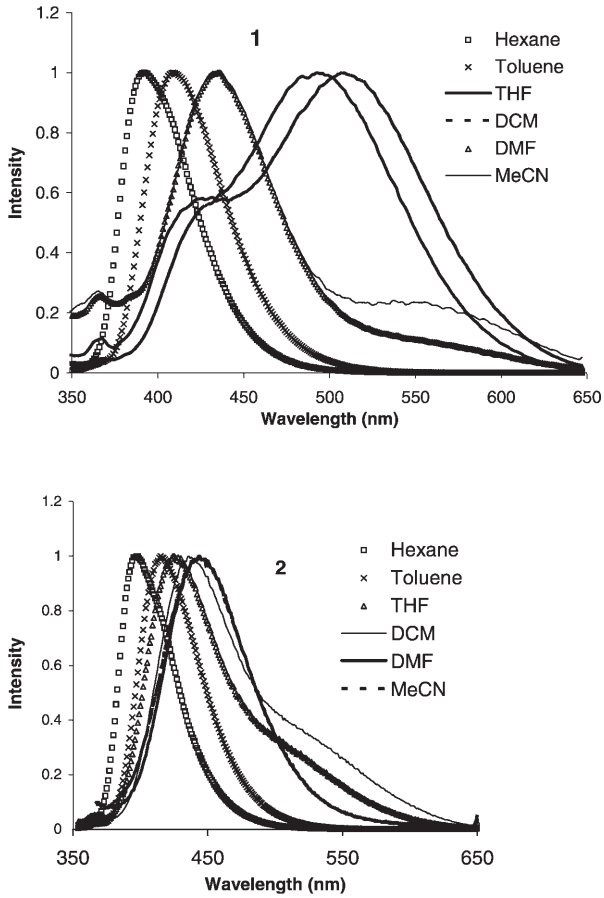

Figure 4. The normalized emission spectra of **1** (top) and **2** (bottom) in various solvents ($\approx 1.0\times10^{-5}$ M).

Table 2. Electrochemical and HOMO–LUMO data.[a]

	E_{ox} [V]	E_{red} [V]	HOMO [eV]	LUMO [eV]	LUMO from optical gap [eV]	Optical energy gap [eV]	Electrochem energy gap [eV]	Solvent (oxidation/reduction)
BNPB	1.03	−1.88	−5.30	−2.44	−2.44	2.88	2.86	DCM/THF
1	1.10	N/A	−5.40	N/A	−2.20	3.20	N/A	DCM/DMF
2	1.10	N/A	−5.40	N/A	−2.20	3.10	N/A	DCM/DMF
3	1.00	N/A	−5.30	N/A	−2.20	3.10	N/A	DCM/DMF
sBN	1.10	−1.75	−5.30	−2.48	−2.29	3.04	2.82	DMF/DMF
BN	1.15	−1.74	−5.35	−2.49	−2.22	3.13	2.86	DMF:THF/DMF:THF

[a] N/A = not applicable.

relationship with solvent polarity as system **A** molecules do. For example, the emission maximum of **1** and **3** in DMF and CH_3CN is at much shorter wavelengths than those in less polar solvents such as THF and CH_2Cl_2. In addition, a shoulder peak is evident in some of the emission spectra of **1** and **3**. In CH_2Cl_2 and THF, this shoulder peak appears at a shorter wavelength from the main peak, while in DMF and CH_3CN it appears at a much longer wavelength from the main peak. The appearance of the emission spectra of **2** in various solvents is distinctly different from those of **1** and **3**. In THF and CH_2Cl_2, the emission spectra of **2** have a shoulder peak at $\approx$530 nm, while the main peak appears at $\lambda_{max} = \approx$432 nm as shown in Figure 4 (bottom). The other notable difference between system **A** and **B** molecules is that the former are highly efficient emitters with very high emission quantum efficiencies (e.g., BNPB, $\Phi = 0.82$ in CH_2Cl_2 and 0.48 in DMF) and the latter are much weaker emitters (e.g. **1**, $\Phi = 0.27$ in CH_2Cl_2 and 0.07 in DMF).

The emission spectra of **1**–**3** are in sharp contrast to that of sBN, which displays a single and well-defined emission peak in various solvents that shifts to lower energy with increasing solvent polarity, as the linear molecule BNPB does (Figure 5). The BN compound, however, does display a

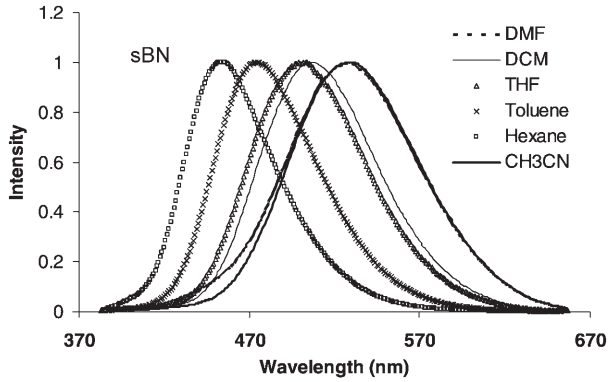

Figure 5. The normalized emission spectra of sBN in various solvents ($\approx 1.0 \times 10^{-5}$ M).

broad emission band with a visible shoulder peak in some solvents (see Supporting Information). Nonetheless, the emission spectra of BN are consistently dominated by the long wavelength peak. The clues that provide some insights into the contrasting luminescent properties of **1**–**3**, sBN, and BN came from our investigation on luminescent change of these molecules upon the addition of fluoride ions.

Luminescent response to fluoride ions: Yamaguchi, Gabbai, Jäkle, and others have shown recently that three-coordinate boron compounds can have highly selective response to fluoride ions that can be monitored either by the absorption spectral change or the emission spectral change if the compound is luminescent.[3] In a preliminary communication[4] we reported that the linear BNPB molecule experiences fluorescent quenching, while the U-shaped molecule BN experiences emission color change from green to blue and a drastic emission intensity enhancement upon the addition of fluoride ions in CH_2Cl_2 or THF. These previous findings indicate that fluoride ions can be used to probe the structure and the nature of luminescence for system **B** molecules.

The fluorescent titration diagrams for compounds **1** and **2** in THF by NBu_4F are shown in Figure 6 (the titration dia-

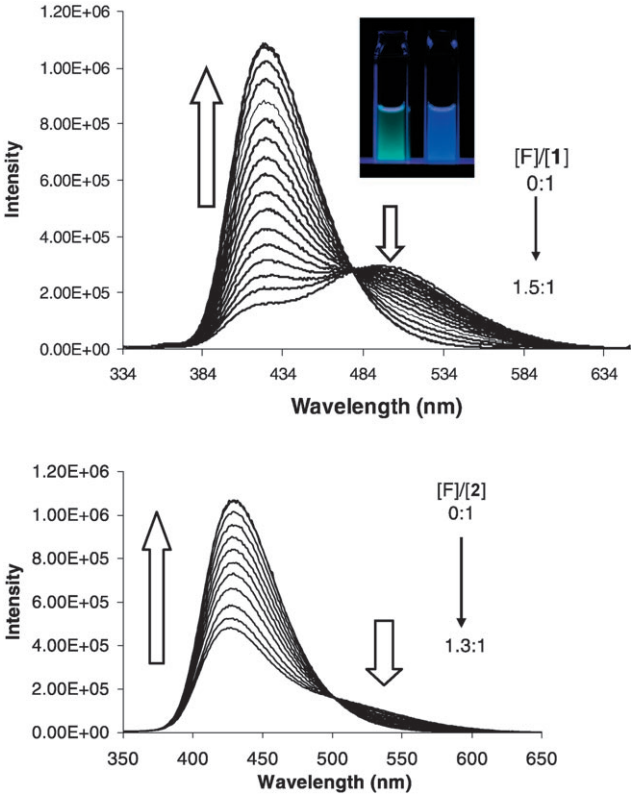

Figure 6. Top: The fluorescent titration diagram of **1** in THF by NBu_4F (1.87×10^{-6} M). Inset: photographs of the solution of **1** before (left) and after the addition of F^- with UV lamp excitation. Bottom: The fluorescent titration diagram of **2** in THF by NBu_4F (1.67×10^{-6} M).

gram for **3** is provided in the Supporting Information). The titration diagrams of **1** and **3** have similar appearance: the addition of the fluoride ion causes the shift of the emission band at $\lambda_{max} = \approx$500 to $\approx$428 nm, and a visual change of color from blue-green to blue as shown by the photographs in Figure 6. More importantly the emission intensity experienced a dramatic increase after the addition of F^-. The difference between **1** and **3** is that **1** needs approximately one equivalent of F^- to reach saturation while **3** needs approximately two equivalents of F^- to reach saturation as shown by the Stern-Volmer plots in Figure 7, which is consistent with the number of boron acceptor sites in these two molecules. There are in fact two isosbestic points in the titration diagram of **3** at 499 and 477 nm (see Supporting Information), indicative of the formation of both $[\mathbf{3}\cdot F]^-$ and $[\mathbf{3}\cdot F_2]^{2-}$ species.[12] For compound **2** the addition of fluoride enhances the emission intensity at 432 nm and decreases the intensity of the shoulder peak at 510 nm and the saturation point is reached after the addition of one equivalent of F^-. The fact

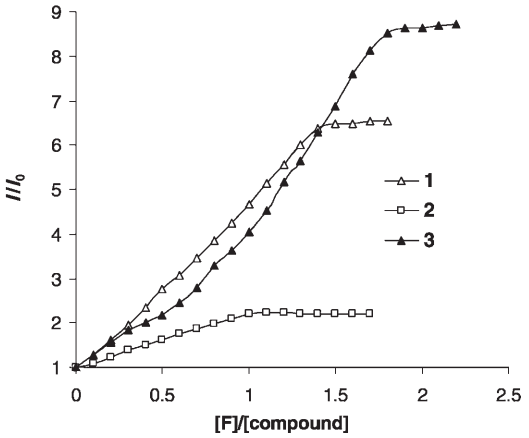

Figure 7. The Stern–Volmer plots of **1–3** (intensity ratio of the emission peak at the short wavelength, I_2, versus the molar ratio of F^- per compound).

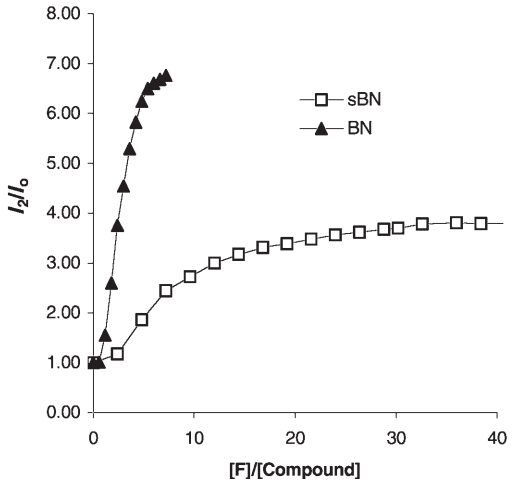

Figure 9. The Stern–Volmer plots of sBN and BN. The I_2/I_1 ratiometric plot shows a similar trend and is provided in the Supporting Information.

that the saturation point was reached with approximately stoichiometric amount of F^- for all three compounds in the V-shaped system **B** supports that these complexes have a strong binding constant to fluoride ions. Due to the strong binding, we have not been able to obtain reliable binding constants for these molecules. The dramatic blue shift of λ_{max} and the enhancement of emission intensity displayed by **1** and **3** upon the addition of fluoride are similar to the behavior of sBN and BN (see Figure 8 and Supporting Information). However, unlike the U-shaped sBN and BN, which require ≈30 and ≈6 equivalents of F^-, respectively, to reach saturation as shown by Figure 9 (the binding constants of F^- for sBN and BN were estimated,[4,12] to be $1.4\times10^4\,M^{-1}$ and $4.0\times10^4\,M^{-1}$, respectively.), the response of compounds **1–3** towards F^- is much more sensitive, making them better candidates as potential sensors for fluorides. Similar to sBN and BN molecules, compounds **1–3** do not show any evident change toward Cl^- or Br^-, as confirmed by NMR competition experiments and fluorescent titration experiments (see Supporting Information).

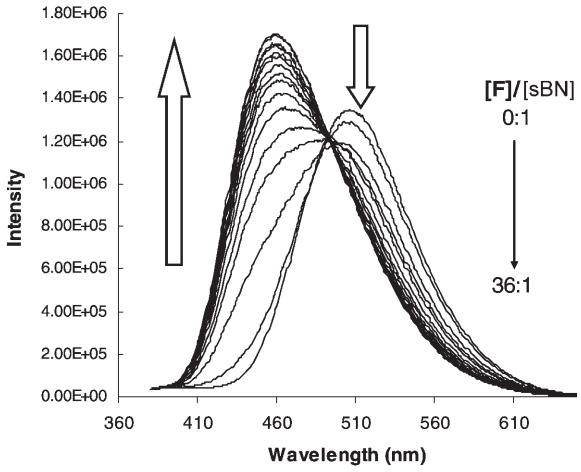

Figure 8. The fluorescent titration diagram of sBN by NBu_4F in CH_2Cl_2 (7.1×10^{-6} M).

Based the fluorescent titration data, we conclude the following:

1) The main emission peak of **1** and **3** at ≈508 nm and the shoulder emission peak of **2** at ≈510 nm in THF (or CH_2Cl_2) originate from B–N charge-transfer transition. The addition of fluoride ions blocks the through-space charge-transfer transition, resulting in quenching of this long wavelength emission peak. This is confirmed by the linear relationship of the Stokes shift of the emission band at the long wavelength with solvent polarity for **1** and **3** (See Supporting Information).
2) The shoulder emission peak of **1** and **3** at ≈430 nm and the main emission peak of **2** at ≈430 nm in THF (or CH_2Cl_2) originate from π–π* transitions localized on the amino leg. Upon blocking of the charge-transfer emission by fluoride ions, the π–π* transitions become the lowest electronic transitions and gain intensity, because of their relatively high emission quantum efficiency. This is supported by the fact that the known hole-transport molecule NPB with a similar structure as the N legs in **1–3** emits at ≈430 nm with a much higher quantum efficiency than those of **1–3** (see Supporting Information). By the same rationale, the dominating emission peak at the long wavelength of the BN molecule can be assigned to charge-transfer emission, while the short wavelength shoulder peak can be assigned to the π–π* transition.
3) Because the main emission peak of **1–3** in DMF and CH_3CN is at the same energy as the emission peak of the F^- adducts of **1–3** in THF, they may have the same origin, that is, π–π* transition. Thus, DMF and CH_3CN solvent molecules must coordinate to the boron center in the same manner as F^- does. However, instead of completely quenching the charge-transfer emission band, DMF or CH_3CN only partially blocks the charge transfer emission, as evidenced by the partially diminished inten-

sity of the charge-transfer band, causing the abnormal spectral shift. DMF molecules are also bound to the boron center in sBN and BN as evidenced by the gradual emission spectral shift in DMF with time to the shorter wavelength (see Figure 10 and Supporting Information).

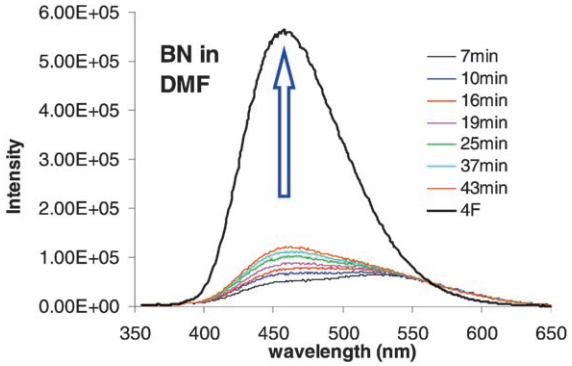

Figure 10. The emission spectra of BN in DMF before and after the addition of four equivalents of F^-.

The slow DMF binding is likely caused by conformational change upon DMF coordination because the DMF binding is even slower in sBN due to increased congestions. (The results of our mechanistic study on this phenomenon will be published in due course.) Nonetheless, DMF clearly cannot compete with fluoride for binding to the boron center as shown by Figure 10 in which the addition of F^- to the solution of BN in DMF causes a huge emission intensity increase (this phenomenon is general for both U-shaped and V-shaped molecules). The dual emission switching mechanism of **1**–**3** in the presence of F^- or donor solvent molecules such as DMF is illustrated in Scheme 4.

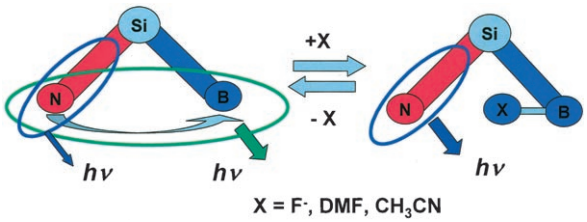

Scheme 4.

Impact of B···N separation distance on charge transfer emission: Figure 4 illustrates that the emission spectra of **1** and **3** in CH_2Cl_2 and THF have very different appearance from that of **2**. For **1** and **3**, the dominating peak is the charge-transfer band, while for **2** the dominating peak is the π–π* transition band. The key difference between **1** (or **3**) and **2** is the separation distance between the donor N atom and the acceptor B atom. For **1** and **3** this distance is ≈10 Å, while for **2** it is 14 Å. Because the further apart the donor and the acceptor are, the more susceptible the through-space charge transfer emission is to collisional/thermal quenching by solvent molecules and hence the lower the emission efficiency,[11,13] the emission spectral difference between **1** (or **3**) and **2** can be attributed to the difference of the B···N separation distance. The greater B···N separation distance in **2** makes the charge-transfer emission much less efficient relative to **1** and **3**. As a consequence, the charge-transfer band of **2** appears as a shoulder peak, instead of the main peak as observed for **1** and **3**. The much weaker response of **2** toward fluoride as shown by Figure 7 is also attributable to the weak charge-transfer emission band of **2** relative to that of **1** and **3**.

The B···N separation distance in the U-shaped sBN and BN is 6.7 and 9.7 Å, respectively. The fact that no dual emission bands were observed for sBN in solution can be attributed to its U-shape and the short B···N distance, which greatly facilitates charge-transfer emission such that it becomes the sole emission peak observed. In contrast, due to the much longer B···N separation distance, the charge-transfer emission in BN is less effective, and as a result both charge-transfer emission and π–π* emission are observed, consistent with the observations for the V-shaped compounds **1**–**3**. The relatively weak binding of sBN to fluoride ions, with respect to BN, can also be considered as a consequence of the shorter B···N separation distance in sBN because it makes F^- binding to the boron center more difficult due to the increased steric congestion in sBN.

Conclusion

Comparison of systems A, B, and C—impact of the spacer: Based on the above results and discussions on system **B** and **C**, we can conclude the following:

Origin of emission: For the linear system **A**, the emission is dictated nearly entirely by B···N charge-transfer emission. The emission efficiency of system **A** is in general very high and attributable to the presence of the conjugated linear linker. For the V-shaped system **B**, dual emission bands from both B–N charge transfer and π–π* transition coexist with a much lower total emission quantum efficiency than system **A**, due to the much decreased efficiency of through-space charge transfer, compared to the through-bond charge transfer in system **A**. The appearance of the emission spectra in system **B** is dependent on the B···N separation distance. With a shorter B···N distance, the emission is dominated by the charge-transfer band, and with a longer B···N distance the emission is dominated by the π–π* transition band. The co-existence of dual emission bands in system **B** is the consequence of the V-shaped Ar_2Si linker that makes the through-space charge-transfer emission possible, but in the meantime, allows rotational freedom of the donor and acceptor groups, thus diminishing the efficiency of through-space charge-transfer emission and activating the π–π* transition. For the U-shaped system **C**, because of the face-to-face geometry and the high rigidity of the donor and accept-

or groups imposed by the 1,10-naphthyl linker, through-space charge-transfer emission dominates, although some contributions from the π–π* transition in the emission band are evident for the BN molecule that has a long B···N separation distance.

Fluoride sensing: For the linear system **A** the addition of F^- causes fluorescent quenching due to the blocking of the boron acceptor site and the high quantum efficiency of the charge-transfer emission. System **A** molecules, in general, have a strong binding constant to F^- and reaches saturation with the addition of less than two equivalents of F^-. For the V-shaped system **B** the addition of fluoride ions quenches the B–N charge-transfer emission band and enhances the π–π* transition band due to the low quantum efficiency of the through-space charge-transfer emission, resulting in both color change and overall fluorescent intensity increase. Molecules in system **B** are therefore "turn-on" sensors for fluoride. System **B** molecules show strong binding to fluoride ions and reach saturation with the addition of approximately stoichiometric amount of fluoride ions, a behavior similar to system **A**. The response of the U-shaped system **C** molecules toward fluoride resembles that of system **B** in that they are all "turn-on" sensors with color change, due to the low quantum efficiency of the charge-transfer emission. However, unlike systems **A** and **B**, molecules in system **C** display in general much weaker binding toward F^-, and the shorter the B···N separation distance, the weaker the binding, which is the consequence of strong steric interactions between the donor and the acceptor legs imposed by the U-shaped geometry.

Taking all factors into consideration, the V-shaped molecules **1** and **3** are the best candidates as sensors for fluoride ions because of their "turn-on" response and their high affinity toward fluoride.

Impact of coordinating solvents: Coordinating solvent molecules such as DMF bind to the boron center in systems **B** and **C**, causing atypical spectral shift with solvent polarity. Despite the coordination to the boron center by solvent molecules such as DMF, the use of **1–3** as fluoride sensors is not hindered in coordinating solvents, because—based on this work and previous work by others—nothing except perhaps CN^- and OH^- can compete with fluoride ions for binding to the sterically protected three-coordinate boron center as in **1–3**, sBN, and BN. The key advantage of our systems **B** and **C**, with respect to other boron-based fluoride-sensing systems, is that they are all "turned on" by fluoride with or without the presence of coordinating solvent molecules. The other advantage of the molecules reported here is that they are all stable toward water and the fluorescence of the boron compounds can be fully restored after the removal of the fluoride ions by water.

In summary, by investigating the photophysical properties and the fluorescent response to solvent molecules and fluoride ions of three distinct groups of organoboron compounds, we have shown that the geometry of the linker and the separation distance between the donor and the acceptor groups in three-coordinate organoboron compounds have a profound impact on the emission pathway and the emission efficiency. Among the three groups of compounds that bear the same donor and acceptor groups, the V-shaped and the U-shaped molecules are most promising as fluoride sensors due to the "turn-on" response. However, the charge-transfer emission in the V-shaped molecules is more sensitive to donor solvent molecules or fluoride anions due to their relatively open geometry than the sterically congested U-shaped molecules. By manipulating the B···N separation distance and the linker's geometry, it is possible to control the fluorescent switching pathway by using fluoride ions, thus achieving highly effective "turn-on" sensors for fluoride ions.

Experimental Section

All starting materials were purchased from Aldrich Chemical Company and were used without further purification. Solvents were freshly distilled over appropriate drying reagents. All syntheses were carried out under a dry nitrogen atmosphere by use of standard Schlenk techniques unless otherwise stated. TLC was carried out on silica gel. Flash chromatography was carried out on silica. ^1H and ^{13}C NMR spectra were recorded on Bruker Avance 300, 400, or 500 MHz spectrometers. Excitation and emission spectra were recorded on a Photon Technologies International QuantaMaster Model 2 spectrometer. Elemental analyses were performed by Canadian Microanalytical Service, Delta, British Columbia (Canada). Cyclic voltammetry was performed on a BAS CV-50W analyzer with a Pt working electrode, Pt auxiliary electrode, and Ag/AgCl reference electrode. All experiments were performed at room temperature with 0.10 M $NBu_4[PF_6]$ as the supporting electrolyte in either CH_2Cl_2 or CH_3CN or DMF. High-resolution mass spectra were obtained using electrospray mode with internal calibrants on an Applied Biosystems/MDS-Sciex QSTAR XL spectrometer. Luminescent quantum yields were determined relative to anthracene in CH_2Cl_2 at 298 K ($\Phi_r = 0.36$). The quantum yields were calculated by previously reported procedures.[5]

Synthesis of intermediate (*p*-1-naphthylphenylaminophenyl)(*p*-Br-phenyl)diphenylsilane (1a): Di(*p*-Br-phenyl)diphenylsilane (4.80 mmol, 2.40 g), 1-naphthylphenylamine (4.00 mmol, 0.880 g), cupric sulfate hydrate (0.20 mmol, 0.050 g), and potassium phosphate (3.16 mmol, 0.670 g) were heated at 240 °C for 48 h under nitrogen. After cooling to ambient temperature, the reaction mixture was dissolved in CH_2Cl_2 (40 mL) and washed by water (3×20 mL). The water layer was separated and extracted with CH_2Cl_2 (3×30 mL). The combined organic layers were dried over $MgSO_4$, and the solvents were evaporated under reduced pressure. The residue was subjected to column chromatography on silica gel (CH_2Cl_2/hexane as eluent) to afford a colorless solid of **1a** in 45% yield. ^1H NMR ($CDCl_3$, 25 °C): $\delta = 7.95$ (d, $J = 8.0$ Hz, 1H), 7.90 (d, $J = 8.0$ Hz, 1H), 7.80 (d, $J = 7.2$ Hz, 1H), 7.51 (m, 8H), 7.39 (m, 12H), 7.23 (m, 2H), 7.15 (m, 2H), 6.97 ppm (m, 3H); ^{13}C NMR ($CDCl_3$, 25 °C): $\delta = 149.79$, 147.53, 142.95, 137.94, 137.21, 136.30, 135.32, 134.14, 133.83, 131.39, 131.03, 129.68, 129.22, 128.47, 127.93, 127.63, 126.93, 126.56, 126.39, 126.24, 124.60, 124.17, 124.05, 122.93, 122.63, 119.68 ppm; HRMS: *m/z* (%): 670.0986 (100) $[M+K]^+$ (calcd: 670.0968).

Synthesis of intermediate (*p*-dimesitylboronylphenyl)(*p*-Br-phenyl)diphenylsilane (2a): A solution of *n*BuLi in hexane (1.6 M, 2.27 mL, 3.63 mmol) was added at −78 °C to a solution of di(*p*-Br-phenyl)diphenylsilane (3.30 mmol, 1.650 g) in Et_2O (50 mL), and the mixture was allowed to reach room temperature over a period of one hour, followed by another hour stirring at room temperature. A solution of dimesitylboron fluoride (0.990 g, 96%, 3.30 mmol) in Et_2O (40 mL) was added to the mixture. The reaction mixture was stirred overnight before water (20 mL) was added. The water layer was separated and extracted with CH_2Cl_2 (3× 30 mL). The combined organic layers were dried over $MgSO_4$, and sol-

vents were evaporated under reduced pressure. The residue was subjected to column chromatography on silica gel (CH_2Cl_2/hexane as eluent) to afford pale yellow solid of **2a** in 50% yield. ^{1}H NMR ($CDCl_3$, 25°C): δ = 7.43 (m, 18H), 6.83 (s, 4H), 2.32 (s, 6H), 2.03 ppm (s, 12H); ^{13}C NMR ($CDCl_3$, 25°C): δ = 140.77, 138.77, 137.91 137.81, 136.41, 136.30, 135.75, 135.06, 133.43, 131.10, 129.85, 128.18, 128.05, 128.00, 127.87, 124.78. 23.43, 3.10 ppm; HRMS: *m*/*z* (%): 701.1834 (100) $[M+K]^+$ (calcd: 701.1813).

Synthesis of intermediate di(*p*-1-naphthylphenylaminophenyl)di(*p*-Br-phenyl)silane (3a): Tetra(*p*-Br-phenyl)silane (3.00 mmol, 1.960 g), 1-naphthylphenylamine (7.50 mmol, 1.290 g), cupric sulfate hydrate (0.33 mmol, 0.083 g) and K_3PO_4 (4.72 mmol, 1.000 g) were heated at 230°C for 48 h under nitrogen. After cooling to ambient temperature, the reaction mixture was dissolved in CH_2Cl_2 (40 mL) and washed with water (3×20 mL). The water layer was separated and extracted with CH_2Cl_2 (3×30 mL). The combined organic layers were dried over $MgSO_4$, and the solvents were evaporated under reduced pressure. The residue was subjected to column chromatography on silica gel (CH_2Cl_2/hexane as eluent) to afford a white solid **3a** in 25%. ^{1}H NMR ($CDCl_3$, 25°C): δ = 7.91 (t, *J* = 8.7 Hz, 4H), 7.79 (d, *J* = 8.4 Hz, 2H), 7.50 (m, 8H), 7.38 (m, 8H), 7.22 (m, 8H), 7.13 (m, 4H), 6.93 ppm (m, 6H); ^{13}C NMR ($CDCl_3$, 25°C): δ = 149.81, 147.45, 142.88, 137.78, 137.06, 135.29, 133.70, 131.35, 131.02, 129.20, 128.45, 127.60, 126.93, 126.55, 126.37, 126.22, 124.62, 124.11, 123.85, 122.94, 122.66, 119.59 ppm; HRMS: *m*/*z* (%): 965.09147 (100) $[M+K]^+$ (calcd: 965.09590).

Synthesis of (*p*-1-naphthylphenylaminophenyl)(*p*-dimesitylboronylphenyl)diphenylsilane (1): A solution of *n*BuLi in hexane (1.6M, 1.15 mL, 1.84 mmol) was added at −78°C to a solution of **1a** (0.950 g, 1.5 mmol) in Et_2O (80 mL), and the mixture was allowed to reach room temperature over a period of one hour, followed by another hour stirring at room temperature. A solution of dimesitylboron fluoride (0.310 g, 96%, 1.0 mmol) in Et_2O (20 mL) was added to the mixture. The reaction mixture was stirred overnight before water (20 mL) was added. The water layer was separated and extracted with CH_2Cl_2 (3×30 mL). The combined organic layers were dried over $MgSO_4$, and the solvents were evaporated under reduced pressure. The residue was subjected to column chromatography on silica gel (CH_2Cl_2/hexane as eluent) to afford pale yellow solid of **1** in 50% yield. ^{1}H NMR ($CDCl_3$, 25°C): δ = 7.96 (d, *J* = 8.4 Hz, 1H), 7.90 (d, *J* = 8.1 Hz, 1H), 7.80 (d, *J* = 8.1 Hz, 1H), 7.55 (m, 6H), 7.49 (m, 4H), 7.37 (m, 10H), 7.23 (m, 2H), 7.14 (m, 2H), 6.98 (m, 3H), 6.82 (s, 4H), 2.31 (s, 6H), 2.02 ppm (s, 12H); ^{13}C NMR ($CDCl_3$, 25°C): δ = 149.66, 147.65, 146.90, 143.04, 141.82, 140.80, 139.06, 138.66, 137.27, 136.35, 135.85, 135.30, 134.97, 134.54, 131.39, 129.50, 129.17, 128.41, 128.14, 127.80, 127.59, 126.82, 126.53, 126.37, 126.20, 124.64, 124.20, 122.80, 122.45, 119.78, 23.44, 21.23 ppm; HRMS: *m*/*z* (%): 840.3577 (100) $[M+K]^+$ (calcd: 840.35991); elemental analysis calcd (%) for $C_{58}H_{52}BNSi$: C 86.87, H 6.54, N 1.75; found: C 86.63, H 7.10, N 1.61.

Synthesis of (*p*-1-naphthylphenylaminobiphenyl)(*p*-dimesitylboronylphenyl)diphenylsilane (2): Degassed EtOH (15 mL), H_2O (15 mL) and toluene (25 mL) was added to a mixture of *p*-1-naphthylphenylamino-phenyl boronic acid (0.680 g, 2.0 mmol), **2a** (0.950 g, 1.43 mol), $[Pd(PPh_3)_4]$ (0.085 g, 0.077 mmol), and Na_2CO_3 (2.50 g). The mixture was stirred and heated at reflux for 3 days. The reaction mixture was dissolved in CH_2Cl_2 (40 mL) and washed with water (3×20 mL). The water layer was separated and extracted with CH_2Cl_2 (3×30 mL). The combined organic layers were dried over $MgSO_4$, and the solvents were evaporated under reduced pressure. The residue was subjected to column chromatography on silica gel (CH_2Cl_2/hexane as eluent) to afford a white solid of **2** in 35% yield. ^{1}H NMR ($CDCl_3$, 25°C): δ = 7.96 (d, *J* = 8.4 Hz, 1H), 7.91 (d, *J* = 8.1 Hz, 1H), 7.80 (d, *J* = 5.7 Hz, 1H), 7.58 (m, 10H), 7.46 (m, 4H), 7.38 (m, 10H), 7.24 (m, 2H), 7.09 (m, 4H), 6.99 (s, 1H), 6.82 (s, 4H), 2.30 (s, 6H), 2.02 ppm (s, 12H); ^{13}C NMR ($CDCl_3$, 25°C): δ = 148.12, 148.07, 143.33, 141.78, 140.80, 138.70, 138.62, 136.84, 136.40, 135.86, 135.32, 135.03, 134.13, 133.58, 131.88, 131.28, 129.64, 128.43, 128.16, 127.90, 127.70, 127.35, 126.65, 126.50, 126.39, 126.20, 125.95, 124.24, 122.33, 122.09, 121.48, 23.44, 21.22 ppm; HRMS: *m*/*z* (%): 916.3878 (100) $[M+K]^+$ (calcd: 916.39121); elemental analysis calcd (%) for $C_{64}H_{56}BNSi\cdot0.7H_2O$: C 86.33, H 6.45, N 1.57; found: C 86.17, H 6.76, N 1.62.

Synthesis of di(*p*-1-naphthylphenylaminophenyl)di(*p*-dimesitylboronylphenyl)silane (3): A solution of *n*BuLi hexane (1.6M, 0.82 mL, 1.31 mmol) was added at −78°C to a solution of **3a** (0.565 g, 0.6 mmol) in Et_2O (45 mL), and the mixture was allowed to reach room temperature over a period of one hour, followed by another hour stirring at room temperature. A solution of dimesitylboron fluoride (0.430 g, 96%, 1.44 mmol) in Et_2O (20 mL) was added to the mixture. The reaction mixture was stirred overnight before water (20 mL) was added. The water layer was separated and extracted with CH_2Cl_2 (3×30 mL). The combined organic layers were dried over $MgSO_4$, and the solvents were evaporated under reduced pressure. The residue was subjected to column chromatography on silica gel (CH_2Cl_2/hexane as eluent) to afford pale yellow solid of **3** in 70% yield. ^{1}H NMR ($CDCl_3$, 25°C): δ = 7.95 (dd, *J* = 8.0, 1.0 Hz, 4H), 7.82 (d, *J* = 8.0 Hz, 2H), 7.53 (d, *J* = 8.0 Hz, 4H), 7.48 (t, *J* = 8.0 Hz, 8H), 7.38 (t, *J* = 8.0 Hz, 4H), 7.33 (t, *J* = 8.0 Hz, 4H), 7.23 (t, *J* = 8.0 Hz, 4H), 7.14 (t, *J* = 8.0 Hz, 4H), 6.97 (m, 6H), 6.83 (s, 8H), 2.33 (s, 12H), 2.02 ppm (s, 24H); ^{13}C NMR (CD_2Cl_2, 25°C): δ = 149.73, 147.64, 142.98, 141.70, 140.70, 139.32, 138.76, 137.10, 135.75, 135.35, 134.85, 131.33, 129.13, 128.40, 128.08, 127.57, 126.80, 126.46, 126.39, 126.20, 124.90, 123.95, 122.76, 122.48, 119.73, 23.12, 20.90 ppm; HRMS: *m*/*z* 1305.624140 (100) $[M+K]^+$ (calcd: 1305.624800); elemental analysis calcd (%) for $C_{92}H_{84}B_2N_2Si\cdot1.3H_2O$: C 85.62, H 6.72, N 2.17; found: C 85.51, H 6.76, N 2.13.

Synthesis of intermediate 1-iodo-8-*p*-dimesitylboryphenylnaphthalene (4a): A solution of *n*BuLi in hexane (3.2 mL, 1.6M, 5.12 mmol) was added to a solution of *p*-bromophenyldimesitylborane, (2.0 g, 4.94 mmol) in THF (50 mL) at −78°C. The mixture was stirred for one hour followed by the addition of anhydrous $ZnCl_2$ (0.75 g, 5.50 mmol). The solution was allowed to warm to room temperature. 1,8-Diiodonaphthalene (3.04 g, 8.00 mmol) and $[Pd(PPh_3)_4]$ (0.23 g, 5 mol%) were added sequentially. The mixture was stirred overnight at room temperature. The solvent was removed and the residue was purified by column chromatography in silica gel. After removing unreacted 1,8-diiodonaphthalene and other impurities by using hexane as the eluent, **4a** was isolated by using CH_2Cl_2/hexane (1:9, v/v) as the eluent (1.34 g, 59% based on the boron starting material). ^{1}H NMR (CD_3Cl): δ = 8.20 (d, *J* = 8.0 Hz, 1H; Ar), 7.92 (d, *J* = 8.0 Hz, 1H; Ar), 7.86 (t, *J* = 5.0 Hz, 1H; Ar), 7.60 (d, *J* = 8.0 Hz, 2H; Ar), 7.50(d, *J*=5.0 Hz, 2H; Ar), 7.35 (d, *J* = 8.0 Hz, 2H; Ar), 7.11 (t, *J* = 8.0 Hz, 1H; Ar), 6.85 (s, 4H; Ar), 2.33 (s, 6H; Me), 2.10 ppm (s, 12H; Me); ^{13}C NMR (CD_3Cl): δ = 144.37, 141.27,140.76, 138.93, 137.78, 131.29, 128.25 (8s, Ar), 23.42, 21.22 ppm (2s, Me); HRMS (TOF-EI+): *m*/*z* calcd for $C_{34}H_{32}BI$ $[M]^+$: 578.1642; found: 578.1650.

Synthesis of 1-(*p*-1-naphthylphenylaminophenyl)-8-*p*-dimesitylborophenylnaphthalene (sBN): A solution of *n*BuLi in hexane (0.35 mL, 1.6M, 0.56 mmol) was added to a solution of iodo-4′-(1-naphthylphenylamino)-benzene (0. 22 g, 0.52 mmol) in THF (20 mL) at −78°C. The mixture was stirred for one hour at −78°C, followed by the addition of $ZnCl_2$ (82 mg, 0.60 mmol). The cooling bath was removed after 40 min, and the reaction mixture was continually stirred at room temperature for 20 min. A mixture of **4a** (0. 30 g, 0.52 mmol) and $Pd(PPh_3)_4$ (30 mg, 0.026 mmol) was added to this solution at −30°C . The solution was allowed to warm to room temperature and was stirred overnight. The solvent was removed and the residue was purified by column chromatography in silica to give sBN as pale yellow microcrystalline solid using CH_2Cl_2/hexane (1:8, v/v) as the eluent (50 mg, 31%). ^{1}H NMR (CD_2Cl_2): δ = 7.81 (brd, *J* = 8.0 Hz, 1H; Ar), 7.79 (brd, *J* = 8.0 Hz, 2H; Ar), 7.67 (d, *J* = 8.0 Hz, 2H; Ar), 7.44(ddd, *J*=8.0, 7.0, 2.0 Hz, 2H; Ar), 7.26–7.36 (m, 6H; Ar), 7.16 (ddd, *J* = 8.0, 7.0, 1.0 Hz, 1H; Ar), 7.10 (brd, *J* = 7.0 Hz, 1H; Ar), 6.99 (brd, *J* = 8.0 Hz, 2H; Ar), 6.95 (brt, *J* = 8.0 Hz, 2H; Ar), 6.72–6.82 (m, 9H; Ar), 6.57 (brs, 2H; Ar), 2.23 (s, 6H; Me), 1.95 ppm (s, 12H; Me); ^{13}C NMR (CD_2Cl_2): δ = 148.94, 148.72, 148.42, 146.92, 143.78, 141.98, 141.13, 140.93, 140.69, 138.80, 138.56, 137.46, 137.05, 136.00, 135.75, 131.54, 131.29,130.82, 130.45, 129.85, 129.60, 129.30, 128.79, 128.76, 128.56, 127.42, 126.62, 126.43, 125.78, 125.46, 124.61, 122.03, 121.89, 121.04 (s, Ar), 24.18 (brs, Me), 21.32 ppm (s, Me); HRMS: calcd for $C_{56}H_{48}BNK$ $[M+K]^+$: 784.3517; found: 784.3525; elemental analysis calcd (%) for $C_{56}H_{48}BN$: C 90.19, H 6.49, N 1.88; found: C 89.54, H 7.00, N 1.86.

Acknowledgements

We thank the Natural Sciences and Engineering Research Council of Canada for financial support.

[1] a) Z. Yuan, N. J. Taylor, R. Ramachandran, T. B. Marder, *Appl. Organomet. Chem.* **1996**, *10*, 305; b) Z. Yuan, J. C. Collings, N. J. Taylor, T. B. Marder, *J. Solid State Chem.* **2000**, *154*, 5; c) Z. Yuan, N. J. Taylor, T. B. Marder, I. D. Williams, S. K. Kurtz, L. T. Cheng, in *Organic Materials for Nonlinear Optics, II* (Eds.: R. A. Hann, D. Bloor), The Royal Society of Chemistry, Cambridge, **1991**, p. 190; d) C. D. Entwistle, T. B. Marder, *Angew. Chem.* **2002**, *114*, 3051; *Angew. Chem. Int. Ed.* **2002**, *41*, 2927; e) C. D. Entwistle, T. B. Marder, *Chem. Mater.* **2004**, *16*, 4574; f) Z. Yuan, N. J. Taylor, T. B. Marder, I. D. Williams, S. K. Kurtz, L. T. Cheng, *J. Chem. Soc. Chem. Commun.* **1990**, 1489; g) Z. Yuan, C. D. Entwistle, J. C. Collings, D. Albesa-Jové, A. S. Batsanov, J. A. K. Howard, N. J. Taylor, H. M. Kaiser, D. E. Kaufmann, S. Y. Poon, W. Y. Wong, C. Jardin, S. Fathallah, A. Boucekkine, J. F. Halet, T. B. Marder, *Chem. Eur. J.* **2006**, *12*, 2758; h) R. Stahl, C. Lambert, C. Kaiser, R. Wortmann, R. Jakober, *Chem. Eur. J.* **2006**, *12*, 2358; i) L. Porrès, M. Charlot, C. D. Entwistle, A. Beeby, T. B. Marder, M. Blanchard-Desce, *Proc. SPIE-Int. Soc. Opt. Eng.* **2005**, *5934*, 92; j) M. Charlot, L. Porrès, C. D. Entwistle, A. Beeby, T. B. Marder, M. Blanchard-Desce, Phys. *Chem. Chem. Phys.*, **2005**, *7*, 600; k) Z. Yuan, N. J. Taylor, Y. Sun, T. B. Marder I. D. Williams, L.-T. Cheng, *J. Organomet. Chem.* **1993**, *449*, 27.

[2] a) T. Noda, Y. Shirota, *J. Am. Chem. Soc.* **1998**, *120*, 9714; b) T. Noda, H. Ogawa, Y. Shirota, *Adv. Mater.* **1999**, *11*, 283; c) Y. Shirota, M. Kinoshita, T. Noda, K. Okumoto, T. Ohara, *J. Am. Chem. Soc.* **2000**,*122*, 1102; d) T. Noda, Y. Shirota, *J. Lumin.* **2000**, *87–89*, 1168; e) M. Kinoshita, H. Kita, Y. Shirota, *Adv. Funct. Mater.* **2002**, *12*, 780; f) H. Kinoshita, K. Okumoto, Y. Shirota, *Chem. Mater.* **2003**, *15*, 1080; g) M. Uchida, Y. Ono, H. Yokoi, T. Nakano, K. Furukawa, *J. Photopolym. Sci. Technol.* **2001**, *14*, 305; h) Y. Shirota, *J. Mater. Chem.* **2000**, *10*, 1, and references therein; i) W. L. Jia, D. R. Bai, T. McCormick, Q. D. Liu, M. Motala, R. Y. Wang, C. Seward, Y. Tao, S. Wang, *Chem. Eur. J.* **2004**, *10*, 994; j) M. Mazzeo, V. Vitale, F. D. Sala, M. Anni, G. Barbarella, L. Favaretto, G. Sotgiu, R. Cingolani, G. Gigli, *Adv. Mater.* **2005**, *17*, 34; k) W. L. Jia, X. D. Feng, D. R. Bai, Z. H. Lu, S. Wang, G. Vamvounis, *Chem. Mater.* **2005**, *17*, 164; l) W. L. Jia, M. J. Moran, Y. Y. Yuan, Z. H. Lu, S. Wang, *J. Mater. Chem.* **2005**, *15*, 3326.

[3] a) S. Yamaguchi, S. Akiyama, K. Tamao, *J. Am. Chem. Soc.* **2000**, *122*, 6335; b) S. Yamaguchi, T. Shirasaka, K. Tamao, *Org. Lett.* **2000**, *2*, 4129; c) S. Yamaguchi, S. Akiyama, K. Tamao, *J. Am. Chem. Soc.* **2001**, *123*, 11372; d) S. Yamaguchi, T. Shirasaka, S. Akiyama, K. Tamao, *J. Am. Chem. Soc.* **2002**, *124*, 8816; e) H. Shiratori, T. Ohno, K. Nozaki, A. Osuka, *Chem. Commun.* **1999**, 2181; f) Y. Kubo, M. Yamamoto, M. Ikeda, M. Takeuchi, S. Shinkai, S. Yamaguchi, K. Tamao, *Angew. Chem.* **2003**, *115*, 2082; *Angew. Chem. Int. Ed.* **2003**, *42*, 2036; g) S. Solé, F. P. Gabbai, *Chem. Commun.* **2004**, 1284; h) M. Melaimi, F. P. Gabbai, *J. Am. Chem. Soc.* **2005**, *127*, 9680; i) A. Sundararaman, M. Victor, R. Varughese, F. Jäkle, *J. Am. Chem. Soc.* **2005**, *127*, 13748; j) K. Parab, K. Venkatasubbaiah, F. Jäkle, *J. Am. Chem. Soc.* **2006**, *128*, 12879; k) S. Aldridge, C. Bresner, I. A. Fallis, S. J. Coles, M. B. Hursthouse, *Chem. Commun.* **2002**, 740; l) Z. Q. Liu, M. Shi, F. Y. Li, Q. Fang, Z. H. Chen, T. Yi, C. H. Huang, *Org. Lett.* **2005**, *7*, 5481; m) C. Bresner, J. K. Day, N. D. Coombs, I. A. Fallis, S. Aldridge, S. J. Coles, M. B. Hursthouse, *Dalton Trans.* **2006**, 3660; n) C. Bresner, S. Aldridge, I. A. Fallis, C. Jones, L.-L. Ooi, *Angew. Chem. Int. Ed.* **2005**, *44*, 3606; o) C. Dusemund, K. R. A. S. Sandanayake, S. Shinkai, *J. Chem. Soc. Chem. Commun.* **1995**, 333; p) H. Yamamoto, A. Ori, K. Ueda, C. Dusemund, S. Shinkai, *Chem. Commun.* **1996**, 407; q) C. R. Cooper, N. Spencer, T. D. James, *Chem. Commun.* **1998**, 1365; r) S. Arimori, M. G. Davidson, T. M. Fyles, T. G. Hibbert, T. D. James, G. I. Kociok-Koehn, *Chem. Commun.* **2004**, 1640.

[4] X. Y. Liu, D. R. Bai, S. Wang, *Angew. Chem.* **2006**, *118*, 5601; *Angew. Chem. Int. Ed.* **2006**, *45*, 5475.

[5] a) N. J. Demas, G. A. Crosby, *J. Am. Chem. Soc.* **1970**, *92*, 7262; b) I. B. Berlman, *Handbook of Fluorescence Spectra of Aromatic Molecules*, Academic Press, **1971**.

[6] A. Klapars, J. C. Antilla, X. Huang, S. L. Buchwald, *J. Am. Chem. Soc.* **2001**, *123*, 7727.

[7] a) N. Miyaura, *Adv. Met.-Org. Chem.* **1998**, *6*, 187, and references therein; b) A. J. Suzuki, *J. Organomet. Chem.* **1999**, *576*, 147, and references therein.

[8] J. Pommerehne, H. Vestweber, W. Guss, R. F. Mahrt, H. Bassler, M. Porsch, J. Daub, J. *Adv. Mater.* **1995**, *7*, 551.

[9] Gaussian 98 (Revision A.6), M. J. Frisch, G. W. Trucks, H. B. Schlegel, G. E. Scuseria, M. A. Robb, J. R. Cheeseman, V. G. Zakrzewski, J. A. Montgomery, R. E. Stratmann, J. C. Burant, S. Dapprich, J. M. Millam, A. D. Daniels, K. N. Kudin, M. C. Strain, O. Farkas, J. Tomasi, V. Barone, M. Cossi, R. Cammi, B. Mennucci, C. Pomelli, C. Adamo, S. Clifford, J. Ochterski, G. A. Petersson, P. Y. Ayala, Q. Cui, K. Morokuma, D. K. Malick, A. D. Rabuck, K. Raghavachari, J. B. Foresman, J. Cioslowski, J. V. Ortiz, B. B. Stefanov, G. Liu, A. Liashenko, P. Piskorz, I. Komaromi, R. Gomperts, R. L. Martin, D. J. Fox, T. Keith, M. A. Al-Laham, C. Y. Peng, A. Nanayakkara, C. Gonzalez, M. Challacombe, P. M. W. Gill, B. G. Johnson, W. Chen, M. W. Wong, J. L. Andres, M. Head-Gordon, E. S. Replogle, J. A. Pople, Gaussian, Inc., Pittsburgh, PA, **1998**.

[10] D. E. Wong, T. H. Dunning, Jr., *J. Chem. Phys.* **1993**, *98*, 1358.

[11] P. Suppan, N. Ghoneim, *Solvatochromism*, The Royal Society of Chemistry, Cambridge, **1997**.

[12] K. A. Connors, *Binding Constants*, Wiley, New York, **1987**.

[13] J. R. Lakowicz, *Principle of Fluorescent Spectroscopy*, 2nd ed., Kluwer Academic, New York, **1999**.

Received: March 4, 2007
Published online: May 16, 2007

